

SIMULATIONS AND EXPERIMENTAL PLANS FOR A HIGH-REPETITION-RATE FIELD-ENHANCED CONDUCTION-COOLED SUPERCONDUCTING RF ELECTRON SOURCE *

O. Mohsen^{1†}, A. McKeown¹, D. Mihalcea¹, R. C. Dhuley², M. I. Geelhoed²
 V. Korampally¹, P. Piot^{1,2}, I. Salehinia¹, J. C. T. Thangaraj²

¹ Northern Illinois University, DeKalb, IL 60115, USA

² Fermi National Accelerator Laboratory, Batavia, IL 60510, USA

Abstract

We present a novel RF design for a field enhanced electron source driven by field emission cathodes. The proposed electron source relies on the enhanced high electric field gradients at the cathode to simultaneously extract and accelerate electrons. The system will be tested in a conduction-cooled superconducting radio-frequency cavity recently demonstrated at Fermilab. In this paper, we present electromagnetic and thermal simulations of the setup that support the feasibility of the design.

INTRODUCTION

Recent developments in Superconducting Radio-Frequency (SRF) technology are foreseen to be the pathway for lower costs and higher performance accelerators [1]. Higher quality-factor structures will lower the cost of both cryogenic infrastructure and operation [2]. New technologies in cryogenic cooling can eliminate the use of cooling fluids and replace it with a simpler, less space-equipping cryocoolers [3,4]. A key component in enabling the production of high-quality beams at low cost and with compact footprints is the electron source. Electron sources, when coupled to SRF, form the main component of the accelerator. Specifically, the design and operation of SRF electron source have so far exclusively relied on the use of photoemission with a low field on the cathode [5]. The use of photoemission sources requires complicated laser system, increasing the cost and the size of the design. Field Emission (FE) offers an appealing alternative due to its simplified setup. Likewise, FE occurs when emitted surfaces are exposed to strong electric fields. In this paper, we present the electromagnetic design and thermal analysis of an experiment aimed at testing the performance of field-emission cathodes in a high repetition-rate SRF electron source.

CONCEPTUAL DESIGN

The overall design of the proposed electron source is based on 650 MHz single cell elliptical cavity presented in

* This work was supported by the US Department of Energy (DOE) under contract DE-SC0018367 with Northern Illinois University. Fermilab is managed by the Fermi Research Alliance, LLC for the U.S. Department of Energy Office of Science Contract number DE-AC02-07CH11359.

† omohsen@niu.edu

Fig. 1(a). The single cell is flanked with 50 mm beam pipes with flanges attached on each side. The flanges incorporate auxiliary instrumentation including an excitation antenna and an electromagnetic-field probe. Since the fields in the beam pipes are decaying fields, the cavity is not ideal for the emission of a high-quality electron bunch. To overcome this limitation, a cylindrical rod with its extremity located in the high-field region is adapted; see Fig. 1(b). The addition

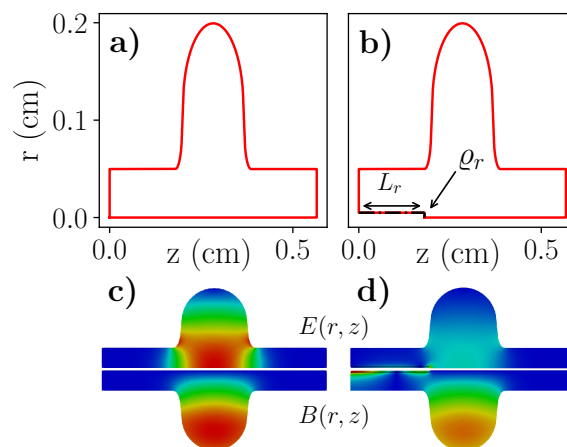


Figure 1: Geometry of the nominal (a) and modified cavity (b) associated with electromagnetic fields [(c) and (d) respectively]. In (c) and (d) the upper and the lower plots corresponds to the normalized electric and magnetic field, respectively.

of the cylindrical rod in the cavity allows the cavity fields on the cathode surface located at the rod extremity. The experimental setup available includes a cryocooler and a solid-state low-level radio-frequency (LLRF) system used to excite the fields. The LLRF setup operates in CW mode at a central frequency of 650 MHz with a full-width bandwidth $\Delta f = 5$ MHz. The cooling capacity of the cryocooler is limited to 1.6 W. Hence, the power dissipated by the formed electron beam should be maintained to a low level.

ELECTROMAGNETIC SIMULATION

For the nominal and the modified cavity, the electromagnetic simulation were performed using SUPERFISH [6] and

Content from this work may be used under the terms of the CC BY 3.0 licence (© 2019). Any distribution of this work must maintain attribution to the author(s), title of the work, publisher, and DOI

OMEGA3P [7]. The two program use different convention for the output parameters. Therefore, we normalize the output parameters based the cooling capacity of the cryocooler ($P_d = 1.6$ W). For instance, the EM fields are renormalized by a multiplicative factor $\sqrt{\frac{P_m}{P_d}}$. Table 1 compares some of the electromagnetic parameters simulated with SUPERFISH and OMEGA3P for the nominal cavity.

Table 1: Comparison Between SUPERFISH and OMEGA3P Electromagnetic Results

parameter	SUPERFISH	OMEGA3P	unit
resonant frequency f	650.057275	650.00135	MHz
stored energy ¹	93.9	$\epsilon_0/2$	J
dissipated power P_d	403.6	2.9×10^{-11}	W
peak field at center	60.9×10^6	26.5	$V m^{-1}$
values renormalized to $P_d = 1.6$ W			
stored energy \mathcal{U}	0.372	0.373	J
peak field at center \hat{E}_0	3.833	3.837	$MV m^{-1}$

¹ by default SUPERFISH normalized the stored energy for an accelerating voltage of 1 MV/m while OMEGA3P stored energy is set to $\epsilon_0/2$.

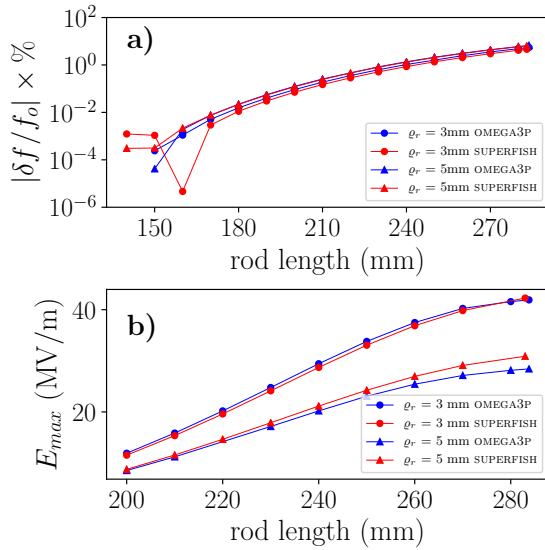


Figure 2: Relative frequency shift (top) and peak electric field at the rod extremity $E_z(\max)$ computed at ($r = 0, z = L_r$) (bottom) as a function of the rod length L_r . The blue and read markers/traces are respectively computed with SUPERFISH and OMEGA3P.

The rod affects the field configuration and resonant frequency [8]. The electromagnetic fields associated with the modified cavity [see Fig. 1(b)] were solved using OMEGA3P. All the conductors (cavity and rod) were taken to be made of niobium, and the rod was parameterized by its length (L_r) and radius (ρ_r). Two cases of radii $\rho_r = [3, 5]$ mm and variable length $L_r \in [140 - 283]$ mm were considered. The shift in the resonance frequency f as a function of the rod parameters appear in Fig. 2(a). The redistribution of the fields inside the cavity leads to an enhanced electric field

at the extremity of the rod along with a higher magnetic field on the rod's side surface; see Fig. 1(c,d). For a given dissipated power, we find that field amplitude at the rod extremity increases with the rod length; see Fig. 2(b). Rod lengths $L_r \leq 220$ mm (resp. $L_r \leq 240$ mm) for a radius $\rho_r = 5$ mm (resp. for a radius $\rho_r = 3$ mm) give an acceptable relative frequency shift within the LLRF-system bandwidth $\delta f / f_0 \leq \Delta f / (2f_0) \approx 0.75\%$. Such geometry produces a peak field of respectively ~ 15 and ~ 30 MV/m on the emitting surface; see Fig. 2(b).

For a cylindrical rod, the maximum field values are attained at the edge of the rod's tip. In order to circumvent this peripheral region to be the site of spurious dark current, we consider smoothing the edges of the rod. We considered rounding the rod edge with a fillet with a radius of curvature R_f . Figure 3 gives the electric fields (axial and radial) at the rod extremity as a function of r for different value of R_f . The later figure indicates that fillets with increasing radii introduce a radial electric field $E_r(r, z = L_r)$ on the rod extremity which is non-vanishing for $r \geq \rho_r - R_f$. We also remark that the maximum radial field does not decrease significantly for radii of curvature $R_f > 1$ mm (and remain approximately at $\sim 1/2$ of the maximum value observed for the sharp edge). It should also be noted that increasing the fillet radius also reduces the usable emitting area. Likewise, the axial electric field $E_z(r, z = L_r)$ is affected by the fillet and start increasing for $r > \rho_r - R_f$. Form these electromagnetic considerations we selected a fillet radius of $R_f = 1$ mm. Likewise, in order to limit the maximum field we chose $L_r \leq 240$ mm and $\rho_r = 5$ mm.

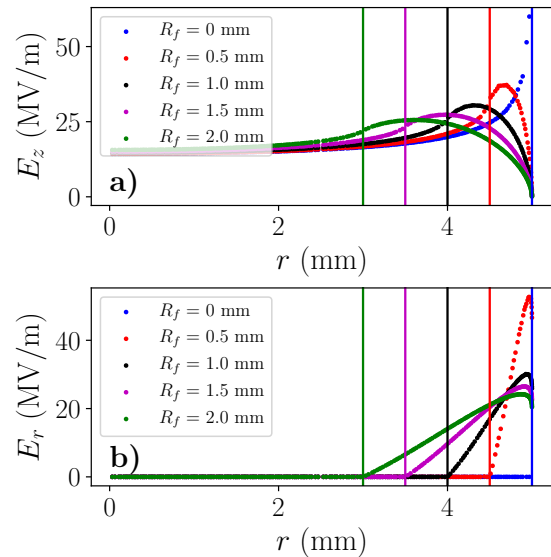


Figure 3: Axial E_z (top) and radial E_r electric field as a function of the radius of curvature of the fillet. The colored vertical lines correspond to the radial distance where the fillet starts.

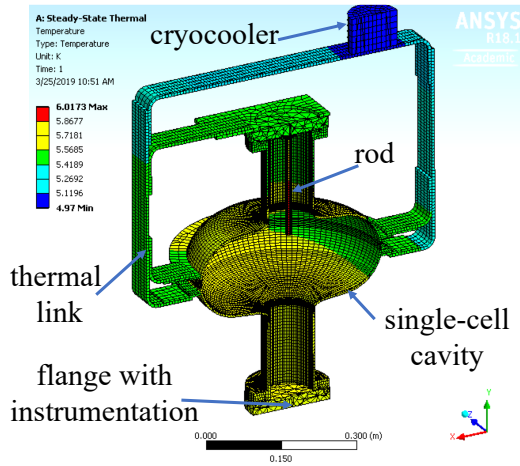


Figure 4: Thermal model of the cavity and auxiliary systems. The colors represent steady-state solution of the temperature (blue and red respectively correspond to 4.97 and 6.02 K). The model was sectioned in half to show the cylindrical rod.

THERMAL SIMULATIONS

A critical aspect of the proposed setup is the design and optimization of the conduction-cooling links to ensure all the niobium masses associated with the cavity and the rod are maintained at a temperature below the critical temperature $T_c = 9.3$ K [9].

The operational temperature of the cavity was simulated using the finite-element analysis (FEA) software ANSYS WORKBENCH 18.1. The thermal model includes the niobium cavity, the cylindrical rod, flanges, and the high-purity-aluminum conduction link; see Fig. 4. The simulations were performed using the steady-state thermal-analysis package given that the time-dependent field have a period $\tau < \frac{1}{650 \times 10^6} \approx 1.5$ ns much faster than any thermal time constants associated with the setup. A fixed temperature boundary condition was used to simulate the cryocooler. Although the cryocooler's operating temperature depends on the experienced heat load, our steady-state simulation assumes steady-state conditions for the heat load of the cryocooler [3]. Additionally, a number of discretized heat-flux boundary conditions, applied to the surfaces of the cavity and cathode mount, were used to simulate the dissipated power. The dissipated power per unit area on the surfaces exposed to the electromagnetic field is given by

$$\frac{dP}{dA} = \frac{1}{2} R_s |\mathbf{H}|^2, \quad (1)$$

where R_s is the surface impedance and \mathbf{H} the magnetic field on the surface. Given the dependence of the surface resistance on the temperature an iterative method was used: the dissipated power $\frac{dP^{(0)}}{dA}$ was evaluated from the electromagnetic simulation and loaded as thermal heat flux in ANSYS for all the surfaces exposed to the electromagnetic field. The resulting temperature $T^{(0)}$ simulated with ANSYS was then

used to compute the dissipated power following the recursive relation (for $n = 0$)

$$\frac{dP^{(n+1)}}{dA} = \frac{1}{2} R_s (T^{(n)}) |\mathbf{H}|^2. \quad (2)$$

The above process was repeated a few times until convergence is achieved by requiring $\epsilon_n \equiv \left| \frac{dP^{(n)}}{dA} - \frac{dP^{(n-1)}}{dA} \right|$ to reach a small value. Figure 5 summarizes the steady-state temperatures reached for the various cases of rod length considered. It indicates that rod with lengths $L_r < 260$ mm and radius $\rho_r = 5$ mm yield a steady-state temperature below the critical temperature. Fig. 5(a) also confirms that the rod tip is the location of the the maximum temperature.

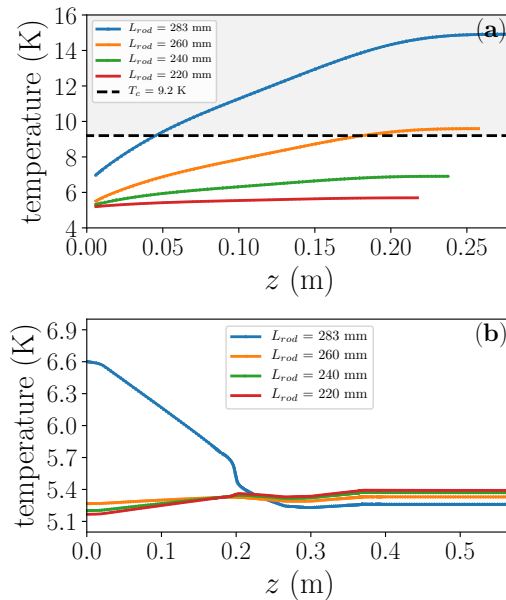


Figure 5: Steady-state temperature reached for the various values of rod length L_r along the rod (a) and external cavity wall (b). The shaded area in (a) indicates region $T \geq T_c$. The ordinate z is defined in Fig 1(b).

CONCLUSION

We presented electromagnetic and thermal simulations in support of a proof-of-principle experiment aimed at testing the operation of field-emission cathode in a conduction-cooled SRF cavity. Such an experiment will be an important step toward the development of compact and simple high-current electron source for a variety of societal applications.

ACKNOWLEDGEMENTS

The authors would like to thank Cho-Kuen Ng and Liling Xiao from SLAC for their useful tips and comments on using OMEGA3P. This research used resources of the National Energy Research Scientific Computing Center which is supported by the Office of Science of the U.S. DOE, Contract No. DE-AC02-05CH11231.

REFERENCES

- [1] R. Kephart *et al.*, “Srf compact accelerator for industry and society,” in *Proceedings of SRF2015, Whistler, BC, Canada*, pp. 1467–1469, 2015.
- [2] D. Gonnella *et al.*, “Nitrogen-doped 9-cell cavity performance in a test cryomodule for lcls-ii,” *Journal of Applied Physics*, vol. 117, no. 2, p. 023908, 2015.
- [3] R. Dhuley, M. Geelhoed, and J. Thangaraj, “Thermal resistance of pressed contacts of aluminum and niobium at liquid helium temperatures,” *Cryogenics*, vol. 93, pp. 86–93, 2018.
- [4] R. Dhuley *et al.*, “Thermal link design for conduction cooling of srf cavities using cryocoolers,” *IEEE Transactions on Applied Superconductivity*, 2019.
- [5] P. Piot *et al.*, “Operation of an ungated diamond field-emission array cathode in a l-band radiofrequency electron source,” *Appl. Phys. Lett.*, vol. 104, p. 263504, 2014.
- [6] M. Menzel and H. K. Stokes, “Users guide for the poison/superfish group of codes,” tech. rep., Los Alamos National Lab., NM (United States), 1987.
- [7] L.-Q. Lee *et al.*, “Omega3p: A parallel finite-element eigenmode analysis code for accelerator cavities,” tech. rep., Stanford Linear Accelerator Center (SLAC), 2009.
- [8] J. C. Slater, “Microwave electronics,” *Reviews of Modern Physics*, vol. 18, no. 4, p. 441, 1946.
- [9] H. Padamsee, J. Knobloch, T. Hays, *et al.*, *RF superconductivity for accelerators*, vol. 2011. Wiley Online Library, 2008.